

SILVERRUSH. IX. Ly α Intensity Mapping with Star-Forming Galaxies at $z = 5.7$ and 6.6 :
Ly α Emission Extended at > 150 comoving kpc Beyond the Virial-Radius Scale of Galaxy Dark Matter Halos

RYOTA KAKUMA,¹ MASMI OUCHI,^{1,2} YUICHI HARIKANE,³ AKIO K. INOUE,⁴ YUTAKA KOMIYAMA,^{3,5} HARUKA KUSAKABE,⁶
CHIEN-HSIU LIU,⁷ YUICHI MATSUDA,^{3,5} YOSHIKI MATSUOKA,⁸ KEN MAWATARI,¹ RIEKO MOMOSE,⁹ YOSHIAKI ONO,¹
TAKATOSHI SHIBUYA,¹⁰ AND YOSHIAKI TANIGUCHI¹¹

¹*Institute for Cosmic Ray Research, The University of Tokyo, 5-1-5 Kashiwanoha, Kashiwa, Chiba 277-8582, Japan*

²*Kavli Institute for the Physics and Mathematics of the Universe (Kavli IPMU, WPI), The University of Tokyo, 5-1-5 Kashiwanoha, Kashiwa, Chiba 277-8583, Japan*

³*National Astronomical Observatory of Japan, 2-21-1 Osawa, Mitaka, Tokyo 181-8588, Japan*

⁴*Institute for Science and Engineering, Waseda University, 3-4-1, Okubo, Shinjuku, Tokyo 169-8555, Japan*

⁵*Graduate University for Advanced Studies (SOKENDAI), 2-21-1 Osawa, Mitaka, Tokyo 181-8588, Japan*

⁶*Observatoire de Genève, Université de Genève, 51 Ch. des Maillettes, 1290 Versoix, Switzerland*

⁷*National Optical Astronomy Observatory*

⁸*Research Center for Space and Cosmic Evolution, Ehime University, 2-5 Bunkyo-cho, Matsuyama, Ehime 790-8577, Japan*

⁹*Department of Astronomy, Graduate School of Science, The University of Tokyo, 7-3-1 Hongo, Bunkyo, Tokyo 113-0033, Japan*

¹⁰*Kitami Institute of Technology, 165 Koen-cho, Kitami, Hokkaido 090-8507, Japan*

¹¹*The Open University of Japan, Wakaba 2-11, Mihama-ku, Chiba 261-8586, Japan*

(Received XXX; Revised YYY; Accepted ZZZ)

Submitted to ApJ

ABSTRACT

We present results of the cross-correlation Ly α intensity mapping with Subaru/Hyper Suprime-Cam (HSC) ultra-deep narrowband images and Ly α emitters (LAEs) at $z = 5.7$ and 6.6 in a total area of 4 deg^2 . Although overwhelming amount of data quality controls have been performed for the narrowband images and the LAE samples, we further conduct extensive analysis evaluating systematics of large-scale point spread function wings, sky subtractions, and unknown errors on the basis of physically uncorrelated signals and sources found in real HSC images and object catalogs, respectively. Removing the systematics, we carefully calculate cross-correlations between Ly α intensity of the narrowband images and the LAEs. We identify very diffuse Ly α emission with the 3σ (2σ) significance at > 150 comoving kpc (ckpc) far from the LAEs at $z = 5.7$ (6.6), beyond a virial radius of star-forming galaxies with $M_{\text{H}} \sim 10^{11} M_{\odot}$. The diffuse Ly α emission possibly extends up to $1,000$ ckpc with the surface brightness of $10^{-20} - 10^{-19} \text{ erg s}^{-1} \text{ cm}^{-2} \text{ arcsec}^{-2}$. We confirm that the small-scale (< 150 ckpc) Ly α radial profiles of LAEs in our Ly α intensity maps are consistent with those obtained by recent MUSE observations (Leclercq et al. 2017). Comparisons with numerical simulations suggest that the large-scale ($\sim 150 - 1,000$ ckpc) Ly α emission are not explained by unresolved faint sources of neighboring galaxies including satellites, but by a combination of Ly α photons emitted from the central LAE and other unknown sources, such as a cold-gas stream and galactic outflow. We find no evolution in the Ly α radial profiles of our LAEs from $z = 5.7$ to 6.6 , where theoretical models predict a flattening of the profile slope made by cosmic reionization, albeit with our moderately large observational errors.

Keywords: galaxies: formation — cosmology: observations — cosmology: early universe

1. INTRODUCTION

Ly α emission is one of the strongest emission lines in galaxy spectra. The Ly α emission is thus widely used for various studies in astronomy, such for galaxy formation, the circumgalactic medium (CGM), the intergalactic medium (IGM), and large scale structures.

Ly α emitters (LAEs) have been identified up to $z \sim 9$ by deep imaging surveys (e.g. Kashikawa et al. 2006; Ouchi et al. 2008, 2010; Hu et al. 2010; Kashikawa et al. 2011; Konno et al. 2014; Matthee et al. 2015; Santos et al. 2016; Zheng et al. 2017; Ota et al. 2017 and spectroscopic observations (e.g. Deharveng et al. 2008; Adams et al. 2011; Schenker et al. 2014; Cassata et al. 2015; Oesch et al. 2015;

Zitrin et al. 2015; Song et al. 2016; Stark et al. 2017). Statistical studies have revealed the general picture of LAEs’ physical properties. Typical LAEs represent low-mass high- z galaxies (Nagao et al. 2005; Ono et al. 2010a,b; Kashikawa et al. 2012; Harikane et al. 2018b), some of which are thought to be candidates of population III galaxies (Partridge & Peebles 1964).

$\text{Ly}\alpha$ photons are produced in the recombination processes of ionized hydrogen gas (HII), and resonantly scattered in neutral hydrogen (HI) gas surrounding a galaxy (Smith et al. 2018). Recently, extended $\text{Ly}\alpha$ emission around galaxies have been identified. Steidel et al. (2011) and Matsuda et al. (2012) have found that extended $\text{Ly}\alpha$ haloes (LAHs) around high- z star-forming galaxies are ubiquitous. Momose et al. (2014) have made samples of 100-3600 LAEs at $z = 2.2$ -6.6 from narrowband imaging (NB) data, and conducted image stacking with intensive tests for checking the systematics. The LAHs at $z = 2.2$ -6.6 have been identified with exponential scale lengths of ~ 5 -10 physical kpc (pkpc). The Multi-Unit Spectroscopic Explorer (MUSE) on the Very Large Telescope enables us to detect LAHs on the individual basis with no stacking analysis (Wisotzki et al. 2016, 2018). Leclercq et al. (2017) report the detection of LAHs around 145 individual LAEs at $3 \leq z \leq 6$ in the Hubble Ultra Deep Field (HUDF). Leclercq et al. (2017) have conducted two exponential component decomposition of a core and a halo for the $\text{Ly}\alpha$ radial profile on pseudo NB images of the MUSE data, and found 80% of objects show the radial profile of the $\text{Ly}\alpha$ more extended than the one of the UV continuum. Extended $\text{Ly}\alpha$ emission have been found not only around LAEs but also around other types of objects. Martin et al. (2014) and Cantalupo et al. (2014) have revealed quasars with $\text{Ly}\alpha$ emission extended to 250-460 pkpc. This largely-extended $\text{Ly}\alpha$ emission is attributed to fluorescent emission from central quasars.

Recently, studies of intensity mapping analyses have investigated the large-scale matter distribution with $\text{Ly}\alpha$ emission (Chang et al. 2010; Comaschi & Ferrara 2016; Croft et al. 2016, 2018; Kovetz et al. 2017; Chiang et al. 2018). The intensity mapping measures the integrated emission of spectral lines from galaxies and the IGM. Croft et al. (2016, 2018) derive a cross-correlation function between the positions of quasars and $\text{Ly}\alpha$ intensity in Sloan Digital Sky Survey spectra of luminous red galaxies after subtracting best-fitting model galaxy spectra, and detect a signal around quasars on scales of 1-15 h^{-1} comoving Mpc. Quasars are very rare objects unlike galaxies. The strong radiation of quasars ionize the IGM gas around quasars. The environment around quasar is special in the universe. For understanding the galaxy formation, it is important to explore the environment around galaxies. To detect the diffuse emission from large-scale matter distribution around galaxies, we can

make use of data from wide-field surveys and the intensity mapping analysis. In this study, we exploit wide and deep optical Hyper Suprime-Cam (HSC; Miyazaki et al. 2012; see also Miyazaki et al. 2018; Komiyama et al. 2018; Furusawa et al. 2018; Kawanomoto et al. 2018) images obtained by the Subaru Strategic Program (HSC SSP; Aihara et al. 2018b). The HSC SSP survey expends 300 nights of Subaru observing time over 5 years since 2014. The survey consists of three layers; Wide (W), Deep (D), and UltraDeep (UD). In the D and UD layers, NB imaging is carried out with 4 filters (*NB387*, *NB816*, *NB921*, *NB1010*). These NB imaging data allow us to make a large LAE sample and to use as $\text{Ly}\alpha$ 2D intensity maps.

In this paper, we will report a first detection of the $\text{Ly}\alpha$ emission around star-forming galaxies largely extended beyond the dark matter halo (DMH) virial radius ($r_{\text{vir}} \sim 150$ comoving kpc (ckpc) for $M_{\text{h}} \sim 10^{11} M_{\odot}$) at $z = 5.7$ and 6.6 based on the intensity mapping analysis of the cross correlation between $\text{Ly}\alpha$ intensity maps and the positions of LAEs. Using the large $\text{Ly}\alpha$ 2D intensity maps and the large LAE samples obtained by the HSC-SSP NB survey, we investigate the large-scale matter distribution around general star-forming galaxies. This paper has the following structure. In Section 2, we describe our LAE catalogs and images. Section 3 presents our analysis and results. In Section 4, we conduct a test to evaluate systematic errors. We briefly discuss a physical origin of extended $\text{Ly}\alpha$ emission and cosmic reionization in section 5. We summarize our findings in Section 6. Throughout this paper we use AB magnitudes (Oke & Gunn 1983) and adopt the Planck cosmological parameter sets of the TT, TE, EE+lowP+lensing+ext result (Planck Collaboration et al. 2016): $\Omega_{\text{m}} = 0.3089$, $\Omega_{\text{r}} = 0.6911$, $\Omega_{\text{b}} = 0.049$, $h = 0.6774$. In this cosmology, $1''$ corresponds to transverse sizes of 40 (42) ckpc at $z = 5.7$ (6.6).

2. DATA

In this study, we exploit the HSC-SSP NB survey data that is taken with *NB816* and *NB921* filters (Ouchi et al. 2018). The *NB816* (*NB921*) filter has a central wavelength of $\lambda_{\text{c}} = 8177\text{\AA}$ (9215\AA) and an FWHM of $\Delta\lambda = 113\text{\AA}$ (135\AA). The *NB816* and *NB921* filters can identify redshifted $\text{Ly}\alpha$ emission at $z = 5.726 \pm 0.046$ and 6.580 ± 0.056 , respectively. The HSC narrowband filter transmission curves are shown in Figure 1. The depth of NB image data is ~ 25.5 mag and the FWHM size of the point spread function in the HSC images is typically $\sim 0.''8$ (see more details in Shibuya et al. 2018).

2.1. LAE Catalogs

For source catalogs of our intensity mapping analysis, we use the LAE catalogs obtained in the program of ‘‘Systematic Identification of LAEs for Visible Exploration and Reionization Research Using Subaru HSC’’ (SILVERRUSH; Ouchi

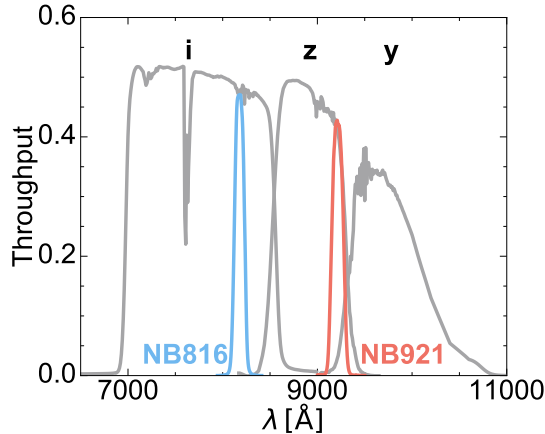


Figure 1. HSC filter transmission curves of the narrowband and broadband filters. The blue (red) line represents the transmission curve of the *NB816* (*NB921*) filter. The gray lines denote the HSC *i*, *z*, and *y* broadband filters.

et al. 2018, Shibuya et al. 2018). The SILVERRUSH LAE catalog is derived from the HSC-SSP survey data whose first data release is presented in Aihara et al. (2018a). This is the largest $z \gtrsim 5$ LAE catalog to date. The details of the SILVERRUSH catalogs are listed in Table 1.

The number of $z = 6.6$ LAEs in UD-SXDS field appears to be smaller than that of the UD-COSMOS field. Shibuya et al. (2018) attribute this difference to the seeing size of the *NB921* images of the UD-SXDS field that is worse than the one of the UD-COSMOS field. Figure 5 of Shibuya et al. (2018) shows that the surface number density of LAEs in the UD-COSMOS field is comparable to those identified in Subaru/Suprime-Cam NB surveys. Though the SILVERRUSH program exploits the HSC-SSP data taken in the D and UD layers, we use only those taken in the UD layer that provides the highest quality data in the HSC SSP survey. Figure 2 displays the sky distribution of the LAEs in the UD layer.

2.2. Images

For an intensity map of the Ly α emission at the redshift same as those of LAEs at $z = 5.7$ (6.6), we use *NB816* (*NB921*) images in the HSC-SSP survey S18A data release. The NB images in the S18A data release is ~ 1 mag deeper than those in the S16A data release. The images in the S18A data release are reduced with HSC pipeline v6.7 (Bosch et al. 2018) that implements an improved sky background subtraction approach. The HSC pipeline v6.7 jointly models and subtracts scattered lights from bright objects and instrumental features crossing all CCDs. In addition, the sky background emission are estimated and subtracted in the mosaic with a grid size of 6000 pixel ($17'$). This new sky subtraction method reduces overfittings and oversubtractions of the sky background made by small scale fluctuations. Although the

Field	Area (deg ²)	m_{lim} (mag)	N_{LAE}	$\log(L_{Ly\alpha}/[\text{erg s}^{-1}])$
(1)	(2)	(3)	(4)	(5)
<i>NB816</i> ($z \sim 5.7$)				
UD-COSMOS	1.97	25.7	201	-
UD-SXDS	1.93	25.5	224	-
Total	3.9	-	425	42.0 - 43.8
<i>NB921</i> ($z \sim 6.6$)				
UD-COSMOS	2.05	25.6	338	-
UD-SXDS	2.02	25.5	58	-
Total	4.07	-	396	42.3 - 44.0

Table 1. (1) Field. (2) Survey Area. (3) Limiting magnitude of the NB image defined by the 5σ detection level in a $1.''5$ diameter circular aperture. (4) Number of the LAEs. (5) The range of LAE Ly α luminosity.

latest S18A data is released very recently (June 2018), we have not selected LAEs from this data.

The NB images contain not only Ly α emission at $z = 5.7$ or 6.6 but also continuum and emission lines that are emitted from low- z sources. The effects from these contaminants can nevertheless be removed by taking a spatial cross-correlation with LAEs because these sources randomly located on the sky respect to the LAEs. The low- z sources only add noise on the cross-correlation between the LAEs and Ly α emission.

Note that we need to mask bright sources on the images to improve the signal to noise ratio (S/N) of the diffuse extended emission. The HSC pipeline sets some flags to each pixel. We do not use pixels with flags of BRIGHT_OBJECT or DETECTED. The BRIGHT_OBJECT flag is given to pixels where nearby very bright objects would affect to the background subtraction or detection. The DETECTED flag is given to the pixels in which sources are detected at the $S/N > 5$ level. With these flags, the pixels in which LAEs are detected are also masked out. We focus on extended Ly α emission at $\geq 1.''5$ separated from the LAEs. This is about two times larger than the size of LAEs on the images that are marginally resolved.

3. ANALYSIS & RESULTS

3.1. Cross-correlation analysis

We derive the angular cross-correlation function between the LAEs and the Ly α intensity $\xi_{IM}(r)$, taking a mean over all LAE-pixel pairs that are separated by r within a certain bin:

$$\xi_{IM}(r) = \frac{1}{N} \sum_i \mu_{r;i}, \quad (1)$$

where $\mu_{r;i}$ is the Ly α intensity in the images at pixel i for the bin r . N is the number of all LAE-pixel pairs separated by r within a certain bin. We note that $\xi_{IM}(r)$ is not the dimensionless cross-correlation function, but the cross-correlation

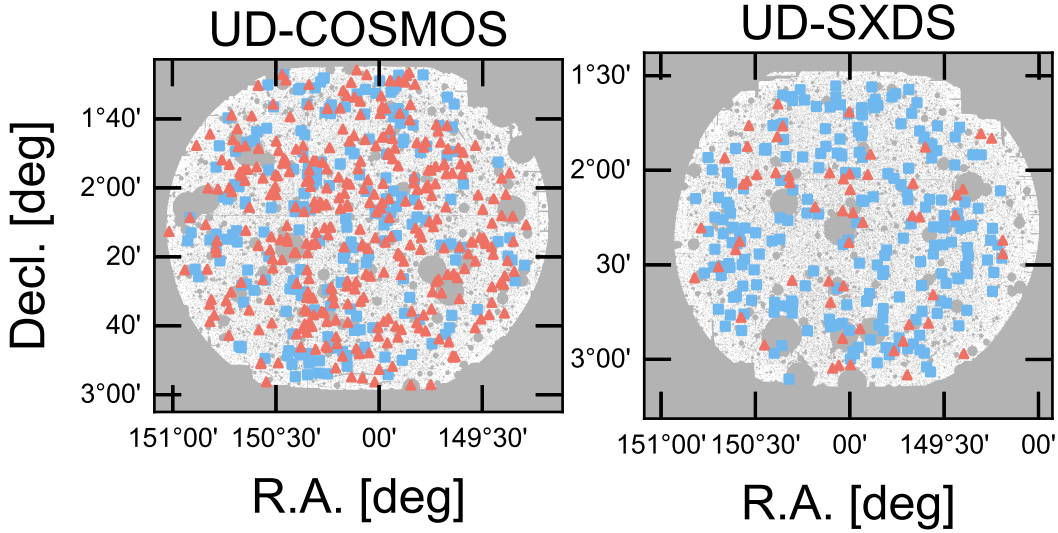


Figure 2. Sky distribution of LAEs in the UD-COSMOS and UD-SXDS fields taken from the SILVERRUSH catalogs. The blue squares and red triangles represent positions of LAEs at $z = 5.7$ and 6.6 , respectively.

function with the unit of intensity. We set six bins logarithmically spaced between $1.''5$ and $40''$. The median distance from one LAE to the closest LAE is $\sim 150''$. We thus rule out the possibility that the closest LAEs contributes to the $\xi_{\text{IM}}(r)$. Statistical uncertainties on the measurements are computed by a bootstrap resampling method. We randomly select LAEs with the number same as that of our LAEs, allowing a duplication. We create 1,000 LAE samples by the random selection, and derive a 1σ standard deviation that is referred to as a 1σ error.

3.2. Tests for systematic errors

There are a number of systematic uncertainties that may produce spurious extended sources in the measurement of diffuse emissions. For example, a largely-extended point-spread function (PSF) and flat-fielding / sky-subtraction systematics may affect the extended profile. We need to carefully evaluate total uncertainties from these systematics. To test the systematics in the cross-correlation between the $\text{Ly}\alpha$ intensity map and the LAEs, we derive a cross-correlation function between the $\text{Ly}\alpha$ intensity map and real foreground objects residing at neither $z = 5.7$ nor 6.6 . We refer to these objects as Non-LAEs. The Non-LAEs are not correlate with $\text{Ly}\alpha$ emission at neither $z = 5.7$ nor 6.6 .

For a catalog of the Non-LAEs, we use the g -band dropout galaxy catalog taken from the ‘‘Great Optically Luminous Dropout Research Using Subaru HSC’’ (GOLDRUSH; [Ono et al. 2018](#), [Harikane et al. 2018a](#)) program. The mean redshift of the Non-LAEs is $z \sim 3.8$. We randomly select the Non-LAEs with the NB magnitude distribution same as that of our LAEs, and make a sample in each field. The systematics like the largely-extended PSF should depend on the

magnitude of the sources. A total of all systematic uncertainties should be the amount of the cross-correlation between the NB images and the Non-LAEs that have the magnitude distribution same as those of LAEs. Because we should reduce the statistical errors of this analysis originated from the Non-LAE samples, we do not match the number but the NB magnitude distribution. The number of the Non-LAEs in the samples are 3-13 times larger than that of the LAEs in each field. We measure the cross-correlation with Non-LAEs in the same manner as the one with LAEs, and evaluate the systematic uncertainties.

3.3. Cross-correlation between LAEs and $\text{Ly}\alpha$ intensity

In Figure 3, we show the cross-correlation between the LAEs (Non-LAEs) and the $\text{Ly}\alpha$ intensity map. The cross-correlations with the Non-LAEs have positive values even at a large scale. It is probably because the images in S18A data release have small residuals that are left in the sky-background subtraction, while the various techniques are applied to remove the residuals. Comparing the cross-correlations of the LAEs and the Non-LAEs, we estimate the amount of the small residuals. Figure 3 indicates that the amplitude of the cross-correlation functions of the LAEs are higher than those of Non-LAEs in each field, albeit with a small excess within the errors in the UD-SXDS field for the LAEs at $z = 5.7$. Because the cross-correlation functions of the LAEs exceed those of the Non-LAEs, we confirm that the systematic uncertainties alone do not explain the cross-correlation functions of the LAEs, but real signals of spatially-extended $\text{Ly}\alpha$ emission.

To evaluate the spatially-extended $\text{Ly}\alpha$ emission quantitatively, we subtract the cross-correlation function of the Non-

LAEs from the one of the LAEs. The uncertainties of the measurements are estimated on the basis of the error propagation. We obtain weighted mean values of the results in the UD-COSMOS and UD-SXDS fields that are calculated with the weights defined by the inverse values of the 1σ errors. In Figure 4, we show the weighted mean values of the cross-correlation functions at $z = 5.7$ and 6.6 . We also display the Ly α radial profile around an LAE at $z = 5.98$, dubbed #547, that is observed with MUSE (Leclercq et al. 2017) in Figure 4. We choose the #547 LAE from the MUSE objects whose Ly α radial profiles are presented in Leclercq et al. (2017), because the redshift of the LAE is the closest to those of the LAEs in our samples. The Ly α luminosity of the #547 LAE is $\log(L_{\text{Ly}\alpha}/[\text{erg s}^{-1}]) = 42.77$, that is comparable to those of LAEs in our samples.

Here, we convert $\xi(r)$ [$\text{erg s}^{-1} \text{cm}^{-2} \text{\AA}^{-1} \text{arcsec}^{-2}$] to the Ly α flux cross-correlation function $\Xi(r)$ [$\text{erg s}^{-1} \text{cm}^{-2} \text{arcsec}^{-2}$] by multiplying the FWHM of NB filter (FWHM_{NB}).

$$\Xi(r) = \xi_{\text{IM}}(r) \times \text{FWHM}_{\text{NB}} \quad (2)$$

In Figure 4, the MUSE observations identify Ly α emission at the small scale of < 150 ckpc beyond the errors. In this scale, the Ly α intensity radial profiles of our results are consistent with those of the MUSE observations both at $z = 5.7$ and 6.6 . Moreover, our results indicate the existence of very faint spatially-extended Ly α emission more largely than the one of the MUSE results, and suggest that Ly α emission extend to ~ 300 (150) ckpc at $z = 5.7$ (6.6) beyond the errors. We estimate the detection confidence levels of the spatially-extended Ly α emission at the scale of > 150 ckpc to be the 2.7σ (2.4σ) level at $z = 5.7$ (6.6). Figure 4 also indicates a hint of the extended Ly α emission up to $\sim 1,000$ ckpc. Based on the halo occupation distribution models, LAEs in our sample are hosted by the DMHs with the average mass of $\log(\langle M_{\text{h}} \rangle / M_{\odot}) = 10.8_{-0.5}^{+0.3}$ ($11.1_{-0.4}^{+0.2}$) at $z = 5.7$ (6.6) with a Ly α duty cycle of 1% or less (Ouchi et al. 2018). The DMH virial radius a galaxy whose halo mass is $\log(M_{\text{h}} / M_{\odot}) = 11$ is $r_{\text{vir}} \sim 150$ ckpc (Mo & White 2002). By the comparison with the DMH virial radius of $r_{\text{vir}} \sim 150$ ckpc, our study has identified the spatially-extended Ly α emission beyond the DMH virial radius (> 150 ckpc) at the 3σ (2σ) level at $z = 5.7$ (6.6).

4. ANALYSIS FOR SYSTEMATICS

We also investigate the cross-correlation between the LAEs and g -band images taken from the HSC-SSP survey S18A data release (Section 2.2). The 5σ limiting magnitude of the g -band images is ~ 27 mag. Because the g -band filter covers a wavelength range shorter than the observed-frame wavelength of Ly α emission at $z = 5.7$ and 6.6 , the LAEs in our samples should not be detected in the g -band

images. We thus expect that there are no signals in the cross-correlation between the LAEs and the g -band images. One can test a reliability of our results with the systematics subtraction (Section 3.3), investigating departures from zero in the cross-correlation between the LAEs and the g -band images. Performing this test, we derive the cross-correlation function between the LAEs and the g -band images in the UD-COSMOS and UD-SXDS fields, respectively, that are corrected for the systematics in the same manner as our results (Section 3.3). Note that the Non-LAE sample consists of g -dropouts whose g -band fluxes are mostly negligibly small. We show a weighted mean value of the results in the UD-COSMOS and UD-SXDS fields in Figure 5. Figure 5 indicates that the cross-correlation function is consistent with zero within the errors, and that there is no significant systematics mimicking the spatially-extended Ly α emission in our results of Figure 4.

5. DISCUSSION

5.1. Extended Ly α emission

By the cross-correlation analysis, we identify the Ly α emission spatially extending beyond the scale of r_{vir} . Theoretical studies predict that HI gas in the CGM and IGM resonantly scatters Ly α photons that escape from the inter-stellar medium (ISM) of star-forming galaxies. Zheng et al. (2010) perform a radiation-hydrodynamic reionization simulation in a cosmological volume, and present a physical model of Ly α emission observed around LAEs. The radiative transfer simulation is conducted to explain the observed properties of LAEs at $z \sim 5.7$ in the Subaru/XMM-Newton Deep Survey (SXDS; Ouchi et al. 2008). This simulation includes physical processes of Ly α photons scattered by the CGM and IGM. On the basis of the simulation, Zheng et al. (2011) present Ly α radial profiles of stacked images of model LAEs in the simulation. The model LAEs are residing in halos with masses of $M_{\text{h}} \sim 10^{11} M_{\odot}$. Figure 6 compares Ly α radial profiles of the simulation results and our observational results for the LAEs at $z = 5.7$. For comparison, we use the simulation results of "the bright half of the sources" presented in Figure 6 of Zheng et al. (2011), because these sources have Ly α luminosities comparable to those of our LAEs identified in the HSC observations.

Zheng et al. (2011) present that the Ly α radial profile of the simulation consists of two components whose Ly α sources are star-forming regions of the LAE (called 'central LAE') and clustered sources around the LAE (called 'clustering'), i.e. neighboring galaxies including satellites. Figure 6 also shows the total Ly α radial profile, a sum of the two-component Ly α radial profiles. Figure 6 indicates that our observational results agree neither with the total profile nor the clustered-source profile. This is because the clustered-source signals are removed by the masking process before

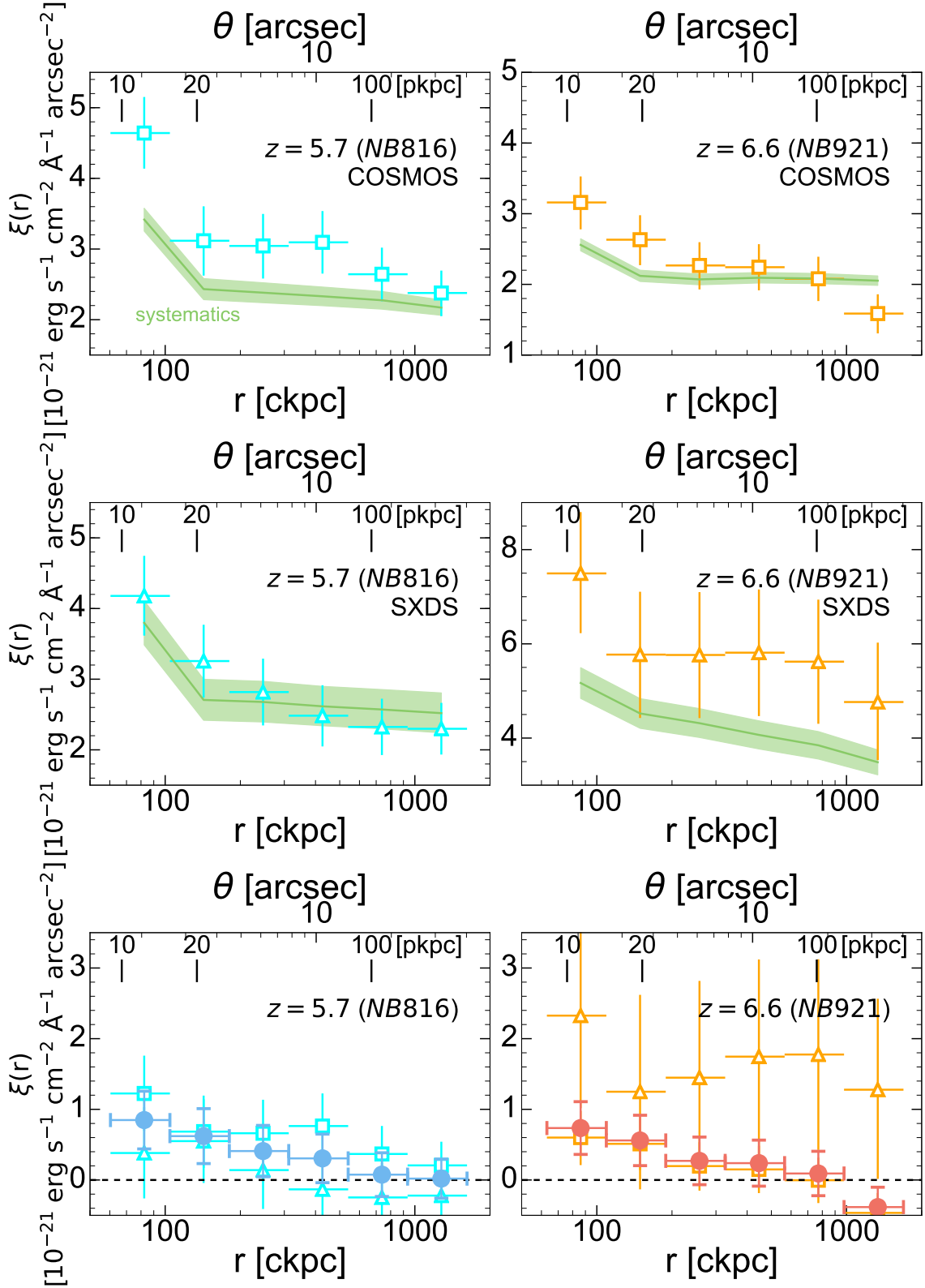


Figure 3. Cross-correlation function between the LAEs (Non-LAEs) and the NB image in each field. The open squares in the top left and right panels show the present the cross-correlation function of the LAEs at $z = 5.7$ and 6.6 in the UD-COSMOS field, respectively. The open triangles in the middle panels are the same as the top panels, but the results for the UD-SXDS field. The green lines denote the cross-correlation functions between the Non-LAEs and the NB image that represent the amount of the total systematics (See text). The green shade regions indicate the 1σ errors. The bottom panels show the cross-correlation functions of the LAEs after subtracting the systematics. The open squares and triangles in the left (right) panel denote the results of $z = 5.7$ (6.6) in the UD-COSMOS and UD-SXDS fields, respectively. The filled circles in the left (right) panel represent the weighted mean values of the results of $z = 5.7$ (6.6) in the UD-COSMOS and UD-SXDS fields that are calculated with the weights defined by the inverse values of the 1σ errors.

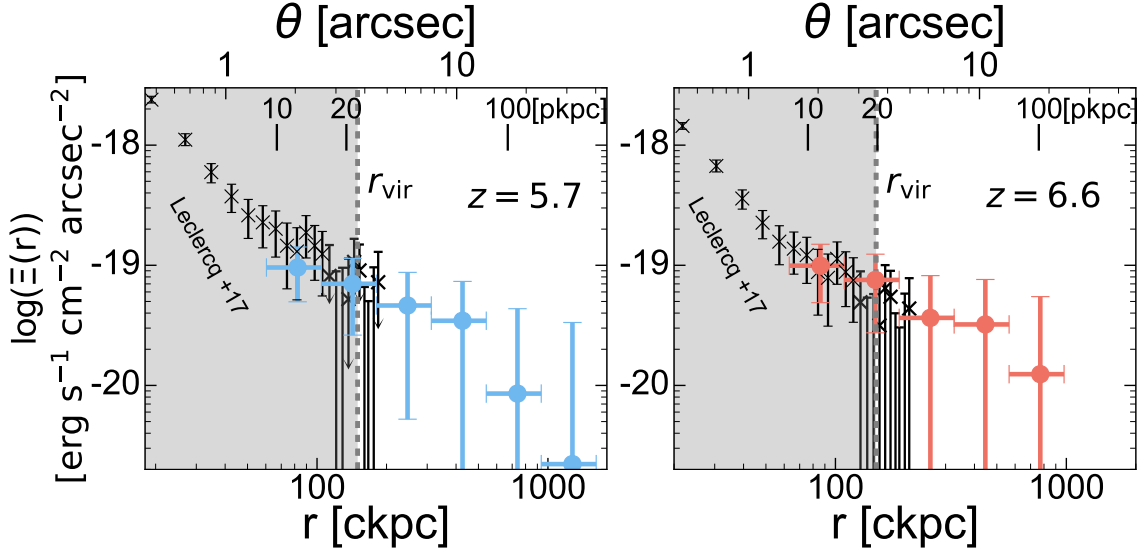


Figure 4. Cross-correlation function between the LAEs and the Ly α emission intensity after subtracting the systematics. The filled circles in the left (right) panel represent the weighted mean of the results in UD-COSMOS and UD-SXDS fields of $z = 5.7$ (6.6). The black crosses correspond to the individual Ly α radial profile at $z = 5.98$ that is taken from the observational results of MUSE (Leclercq et al. 2017, #547). We take into account the dimming effects, and convert the Ly α intensity of the MUSE result. The gray dashed lines show the DMH virial radius (r_{vir}) of the LAEs in our samples whose DMH masses are estimated to be $M_{\text{h}} \sim 10^{11} M_{\odot}$.

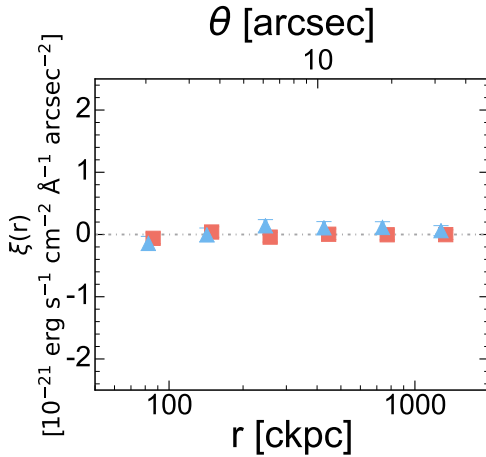


Figure 5. Cross-correlation functions between the LAEs and the g -band images after subtracting the systematics. The blue triangles (red squares) show the cross-correlation function between the LAEs at $z = 5.7$ (6.6) and the g -band images. The gray dotted line corresponds to no correlation.

our cross-correlation measurements (Section 2.2). Here, there is a possibility that faint unresolved sources may not be masked out in our analysis. However, Figure 6 suggests that the Ly α radial profile shapes are different between the clustered source ‘clustering’ and our observational results. In Figure 6, the ‘clustering’ profile decreases only by a factor less than 2 at 150-1000 ckpc, while our observational result profile changes by an order of magnitude beyond the errors. This profile shape difference supports the idea that our ob-

servational results are not explained by the clustered sources including the faint unresolved sources. In Figure 6, the Ly α radial profile of our observational results with the error bars prefers the model of ‘central LAE’ in the simulation. However, the Ly α radial profile of our observational results is higher than the one of the ‘central LAE’ component, albeit with the large observational uncertainties. The Ly α radial profile of the observations exceeding the ‘central LAE’ component may be produced by other physical processes that are not included in the simulation of Zheng et al. (2010), such as a cold-gas stream and galactic outflow that generate Ly α photons by collisional excitation processes.

To understand physical origins of the spatially-extended Ly α emission at the large scale, numerical simulations with various possible physical processes are needed (Sadoun et al. 2019). We also need Ly α intensity mapping measurements with small uncertainties to distinguish the various possible physical models. More Ly α intensity mapping studies should be conducted with the existing instruments including Subaru/HSC. Moreover, we expect to obtain conclusive Ly α intensity mapping results by the on-going and forthcoming projects such as Hobby-Eberly Telescope Dark Energy Experiment (HETDEX; Hill et al. 2008), Wide-Field Infrared Survey Telescope (WFIRST; Spergel et al. 2015), and Spectro-Photometer for the History of the Universe Epoch of Reionization and Ices Explorer (SPHEREx; Doré et al. 2014).

5.2. Cosmic Reionization

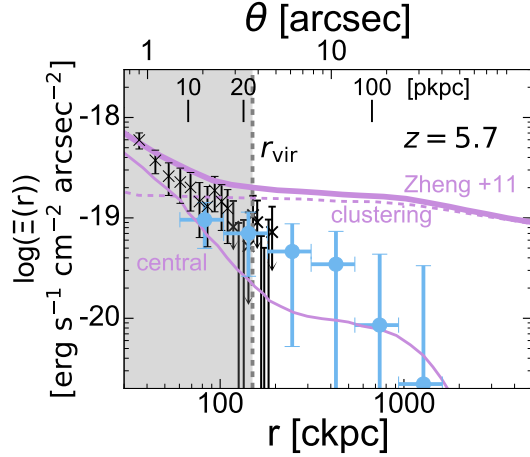


Figure 6. $\text{Ly}\alpha$ emission radial profiles of the observational results that are compared with those are predicted with the radiation-hydrodynamic reionization simulation (Zheng et al. 2011). The thick solid line denotes a radial profile of the stacked $z = 5.7$ LAE images in the simulation (See the text for details about the simulation). The simulated $\text{Ly}\alpha$ radial profile is produced by two sources of $\text{Ly}\alpha$ photons, the central LAE (thin solid line) and the clustered sources around the central LAE (dashed line). The blue circles and the black are same as those in the left panel of Figure 3.

Many observational studies have claimed the increase of the IGM neutral hydrogen fraction x_{HI} with the decrease of the $\text{Ly}\alpha$ luminosity function from $z \sim 6$ to 7 and beyond that can be explained by the increase of the $\text{Ly}\alpha$ damping wing absorption given by the neutral IGM (e.g. Ouchi et al. 2010; Goto et al. 2011; Kashikawa et al. 2011). Jeon-Daniel et al. (2012) predict that the $\text{Ly}\alpha$ radial profile of LAEs flattens towards the early epoch of cosmic reionization with a high x_{HI} , due to the IGM neutral hydrogen scattering $\text{Ly}\alpha$ photons. Because we have the observational data of the $\text{Ly}\alpha$ radial profiles at the epoch of reionization ($z = 6.6$) and the post reionization epoch ($z = 5.7$), we examine whether the flattening is found in our observational data. It should be noted that the $\text{Ly}\alpha$ luminosity ranges of our LAEs at $z = 5.7$ and 6.6 are comparable, $\log(L_{\text{Ly}\alpha}/[\text{erg s}^{-1}]) = 42.0 - 43.8$ and $42.3 - 44.0$, respectively (Konno et al. 2018). The difference between the median values of the $\text{Ly}\alpha$ luminosity of the LAEs at $z = 5.7$ and 6.6 is small (within a factor of 3). Figure 7 compares our observational results at $z = 5.7$ and 6.6. Here we apply corrections for the surface brightness dimming effect in our $z = 6.6$ results, and carry out the comparison at $z = 5.7$. Figure 7 indicates that our observational results at $z = 5.7$ and 6.6 are similar, and that there is no signature of the flattening of the $\text{Ly}\alpha$ radial profile towards high z beyond the errors. Because the error bars, especially at a large scale, of our observational results are probably too large to identify the $\text{Ly}\alpha$ radial profile flattening caused by the cosmic reionization, one should investigate a $\text{Ly}\alpha$ radial profile

slope with the large observational data that will be taken by the on-going and forthcoming programs such as HETDEX, WFIRST, and SPHEREx discussed in Section 5.1.

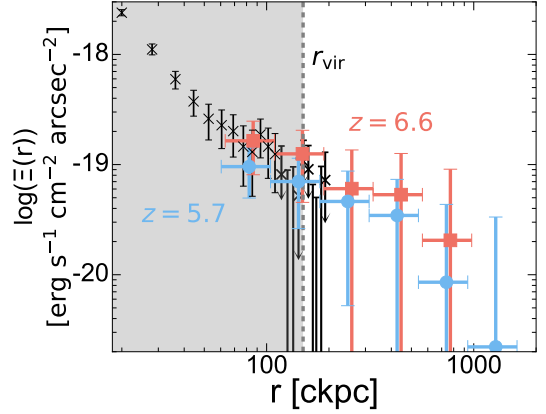


Figure 7. Comparison between the cross-correlation functions of the LAEs at $z = 5.7$ and 6.6. The blue circles and red squares represent the $\text{Ly}\alpha$ cross-correlation functions at $z = 5.7$ and 6.6, respectively. We match the $\text{Ly}\alpha$ radial profile at $z = 6.6$ to the one at $z = 5.7$, correcting for the cosmological surface brightness dimming effect.

6. SUMMARY

In this paper, we report the first detection of the $\text{Ly}\alpha$ emission around the star-forming galaxies largely extended beyond the DMH virial radius ($r_{\text{vir}} \sim 150$ ckpc for $M_{\text{h}} \sim 10^{11} M_{\odot}$) at $z = 5.7$ and 6.6 based on the Subaru/HSC intensity mapping analysis of the cross correlation between the $\text{Ly}\alpha$ intensity map and the positions of LAEs. The major results of this paper are summarized below.

1) Using the largest $z \gtrsim 5$ LAE catalogs to date and the large-area (~ 4 deg²) NB imaging data, we conduct the cross-correlation intensity mapping analysis with the LAEs and the $\text{Ly}\alpha$ intensity map. We conduct extensive analyses evaluating systematics of large-scale PSF wings, sky subtractions, and unknown errors. Confirming that our $\text{Ly}\alpha$ cross-correlations corrected for the systematics produce no spurious detections by the careful tests (Section 4), we have identified very diffuse $\text{Ly}\alpha$ emission at the 3σ (2σ) significance level at the distance of > 150 comoving kpc (ckpc) from the LAEs at $z = 5.7$ (6.6), beyond a virial radius of star-forming galaxies with $M_{\text{h}} \sim 10^{11} M_{\odot}$. The diffuse $\text{Ly}\alpha$ emission possibly extends up to 1,000 ckpc with the surface brightness of $10^{-20} - 10^{-19}$ erg s⁻¹ cm⁻² arcsec⁻². In this analysis, we confirm that the small-scale (< 150 ckpc) $\text{Ly}\alpha$ radial profiles of LAEs in our $\text{Ly}\alpha$ intensity maps are consistent with those obtained by recent MUSE observations (Leclercq et al. 2017).

2) Comparisons with numerical simulations suggest that the large-scale ($\sim 150 - 1,000$ ckpc) $\text{Ly}\alpha$ emission are not

explained by unresolved faint sources of neighboring galaxies including satellites, but by a combination of Ly α photons emitted from the central LAE and other unknown sources, such as a cold-gas stream and galactic outflow.

3) Although theoretical studies predict that the Ly α radial profile is flattened towards the early epoch of cosmic reionization, we find no evolution in the Ly α radial profiles of our LAEs from $z = 5.7$ to 6.6 . However, the moderately large errors may not allow us to identify the flattening of the Ly α radial profiles towards high redshift.

The evolution of the Ly α radial profiles at the EoR should be investigated by very large-area surveys with the on-going and forthcoming programs such with Subaru/HSC, HETDEX, WFIRST, and SPHEREx.

ACKNOWLEDGMENTS

The Hyper Suprime-Cam (HSC) collaboration includes the astronomical communities of Japan and Taiwan, and Princeton University. The HSC instrumentation and software were developed by the National Astronomical Observatory of Japan (NAOJ), the Kavli Institute for the Physics and Mathematics of the Universe (Kavli IPMU), the University of Tokyo, the High Energy Accelerator Research Organization (KEK), the Academia Sinica Institute for Astronomy and Astrophysics in Taiwan (ASIAA), and Princeton University. Funding was contributed by the FIRST program from Japanese Cabinet Office, the Ministry of Education, Culture, Sports, Science and Technology (MEXT), the Japan Society for the Promotion of Science (JSPS), Japan Science and Technology Agency (JST), the Toray Science Foundation, NAOJ, Kavli IPMU, KEK, ASIAA, and Princeton University. The *NB816* filter was supported by Ehime

University (PI: Y. Taniguchi). The *NB921* filter was supported by KAKENHI (23244025) Grant-in-Aid for Scientific Research (A) through the Japan Society for the Promotion of Science (PI: M. Ouchi). This paper makes use of software developed for the Large Synoptic Survey Telescope. We thank the LSST Project for making their code available as free software at <http://dm.lsst.org>. The Pan-STARRS1 Surveys (PS1) have been made possible through contributions of the Institute for Astronomy, the University of Hawaii, the Pan-STARRS Project Office, the Max-Planck Society and its participating institutes, the Max Planck Institute for Astronomy, Heidelberg and the Max Planck Institute for Extraterrestrial Physics, Garching, The Johns Hopkins University, Durham University, the University of Edinburgh, Queens University Belfast, the Harvard-Smithsonian Center for Astrophysics, the Las Cumbres Observatory Global Telescope Network Incorporated, the National Central University of Taiwan, the Space Telescope Science Institute, the National Aeronautics and Space Administration under Grant No. NNX08AR22G issued through the Planetary Science Division of the NASA Science Mission Directorate, the National Science Foundation under Grant No. AST-1238877, the University of Maryland, and Eotvos Lorand University (ELTE). This work is supported by World Premier International Research Center Initiative (WPI Initiative), MEXT, Japan, and KAKENHI (15H02064, 17KK0098, 17H01110, 17H01114 and 17H04831) Grant-in-Aid for Scientific Research (A) through Japan Society for the Promotion of Science. Based on data collected at the Subaru Telescope and retrieved from the HSC data archive system, which is operated by Subaru Telescope and Astronomy Data Center at National Astronomical Observatory of Japan.

REFERENCES

- Adams, J. J., Blanc, G. A., Hill, G. J., et al. 2011, *The Astrophysical Journal Supplement Series*, 192, 5
- Aihara, H., Armstrong, R., Bickerton, S., et al. 2018a, *Publications of the Astronomical Society of Japan*, 70, doi:10.1093/pasj/psx081
- Aihara, H., Arimoto, N., Armstrong, R., et al. 2018b, *Publications of the Astronomical Society of Japan*, 70, doi:10.1093/pasj/psx066
- Bosch, J., Armstrong, R., Bickerton, S., et al. 2018, *Publications of the Astronomical Society of Japan*, 70, doi:10.1093/pasj/psx080
- Cantalupo, S., Arrigoni-Battaia, F., Prochaska, J. X., Hennawi, J. F., & Madau, P. 2014, *Nature*, 506, 63
- Cassata, P., Tasca, L. A. M., Le Fèvre, O., et al. 2015, *Astronomy & Astrophysics*, 573, A24
- Chang, T. C., Pen, U. L., Bandura, K., & Peterson, J. B. 2010, *Nature*, 466, 463
- Chiang, Y.-K., Ménard, B., & Schiminovich, D. 2018, arXiv:1810.00885
- Comaschi, P., & Ferrara, A. 2016, *Monthly Notices of the Royal Astronomical Society*, 463, 3078
- Croft, R. A. C., Miralda-Escudé, J., Zheng, Z., Blomqvist, M., & Pieri, M. 2018, *Monthly Notices of the Royal Astronomical Society*, 481, 1320
- Croft, R. A. C., Miralda-Escudé, J., Zheng, Z., et al. 2016, *Monthly Notices of the Royal Astronomical Society*, 457, 3541
- Deharveng, J., Small, T., Barlow, T. A., et al. 2008, *The Astrophysical Journal*, 680, 1072
- Doré, O., Bock, J., Ashby, M., et al. 2014, arXiv:1412.4872
- Furusawa, H., Koike, M., Takata, T., et al. 2018, *Publications of the Astronomical Society of Japan*, 70, doi:10.1093/pasj/psx079

- Goto, T., Utsumi, Y., Hattori, T., Miyazaki, S., & Yamauchi, C. 2011, *Monthly Notices of the Royal Astronomical Society: Letters*, 415, L1
- Harikane, Y., Ouchi, M., Ono, Y., et al. 2018a, *Publications of the Astronomical Society of Japan*, 70, doi:10.1093/pasj/psx097
- Harikane, Y., Ouchi, M., Shibuya, T., et al. 2018b, *The Astrophysical Journal*, 859, 84
- Hill, G. J., Gebhardt, K., Komatsu, E., et al. 2008, 399, 115
- Hu, E. M., Cowie, L. L., Barger, A. J., et al. 2010, *The Astrophysical Journal*, 725, 394
- Jeerson-Daniel, A., Ciardi, B., Maio, U., et al. 2012, *Monthly Notices of the Royal Astronomical Society*, 424, 2193
- Kashikawa, N., Shimasaku, K., Malkan, M. A., et al. 2006, *The Astrophysical Journal*, 648, 7
- Kashikawa, N., Shimasaku, K., Matsuda, Y., et al. 2011, *The Astrophysical Journal*, 734, 119
- Kashikawa, N., Nagao, T., Toshikawa, J., et al. 2012, *The Astrophysical Journal*, 761, 85
- Kawanomoto, S., Uruguchi, F., Komiyama, Y., et al. 2018, *Publications of the Astronomical Society of Japan*, 70, doi:10.1093/pasj/psy056
- Komiyama, Y., Obuchi, Y., Nakaya, H., et al. 2018, *Publications of the Astronomical Society of Japan*, 70, doi:10.1093/pasj/psx069
- Konno, A., Ouchi, M., Ono, Y., et al. 2014, *The Astrophysical Journal*, 797, 16
- Konno, A., Ouchi, M., Shibuya, T., et al. 2018, *Publications of the Astronomical Society of Japan*, 70, doi:10.1093/pasj/psx131
- Kovetz, E. D., Viero, M. P., Lidz, A., et al. 2017, arXiv:1709.09066
- Leclercq, F., Bacon, R., Wisotzki, L., et al. 2017, *Astronomy & Astrophysics*, 608, A8
- Martin, D. C., Chang, D., Matuszewski, M., et al. 2014, *The Astrophysical Journal*, 786, 106
- Matsuda, Y., Yamada, T., Hayashino, T., et al. 2012, *Monthly Notices of the Royal Astronomical Society*, 425, 878
- Matthee, J., Sobral, D., Santos, S., et al. 2015, *Monthly Notices of the Royal Astronomical Society*, 451, 400
- Miyazaki, S., Komiyama, Y., Nakaya, H., et al. 2012, in *Proc. SPIE*, ed. I. S. McLean, S. K. Ramsay, & H. Takami, Vol. 8446 (International Society for Optics and Photonics), 84460Z
- Miyazaki, S., Komiyama, Y., Kawanomoto, S., et al. 2018, *Publications of the Astronomical Society of Japan*, 70, doi:10.1093/pasj/psx063
- Mo, H. J., & White, S. D. M. 2002, *Monthly Notices of the Royal Astronomical Society*, 336, 112
- Momose, R., Ouchi, M., Nakajima, K., et al. 2014, *Monthly Notices of the Royal Astronomical Society*, 442, 110
- Nagao, T., Kashikawa, N., Malkan, M. A., et al. 2005, *The Astrophysical Journal*, 634, 142
- Oesch, P. A., van Dokkum, P. G., Illingworth, G. D., et al. 2015, *The Astrophysical Journal*, 804, L30
- Oke, J. B., & Gunn, J. E. 1983, *Secondary standard stars for absolute spectrophotometry*, Tech. rep.
- Ono, Y., Shimasaku, K., Dunlop, J., et al. 2010a, *The Astrophysical Journal*, 724, 1524
- Ono, Y., Ouchi, M., Shimasaku, K., et al. 2010b, *Monthly Notices of the Royal Astronomical Society*, 402, 1580
- Ono, Y., Ouchi, M., Harikane, Y., et al. 2018, *Publications of the Astronomical Society of Japan*, 70, doi:10.1093/pasj/psx103
- Ota, K., Iye, M., Kashikawa, N., et al. 2017, *The Astrophysical Journal*, 844, 85
- Ouchi, M., Shimasaku, K., Akiyama, M., et al. 2008, *The Astrophysical Journal Supplement Series*, arXiv:0707.3161
- Ouchi, M., Shimasaku, K., Furusawa, H., et al. 2010, *The Astrophysical Journal*, 723, 869
- Ouchi, M., Harikane, Y., Shibuya, T., et al. 2018, *Publications of the Astronomical Society of Japan*, 70, doi:10.1093/pasj/psx074
- Partridge, R. B., & Peebles, P. J. E. 1964, *Astrophysical Journal*, 147, 868
- Planck Collaboration, Ade, P. A. R., Aghanim, N., et al. 2016, *Astronomy & Astrophysics*, 594, A13
- Sadoun, R., Romano-Díaz, E., Shlosman, I., & Zheng, Z. 2019, *Monthly Notices of the Royal Astronomical Society*, 484, 4601
- Santos, S., Sobral, D., & Matthee, J. 2016, *Monthly Notices of the Royal Astronomical Society*, 463, 1678
- Schenker, M. A., Ellis, R. S., Konidaris, N. P., & Stark, D. P. 2014, *The Astrophysical Journal*, 795, 20
- Shibuya, T., Ouchi, M., Konno, A., et al. 2018, *Publications of the Astronomical Society of Japan*, 70, doi:10.1093/pasj/psx122
- Smith, A., Ma, X., Bromm, V., et al. 2018, 59, 39
- Song, M., Finkelstein, S. L., Livermore, R. C., et al. 2016, *The Astrophysical Journal*, 826, 113
- Spergel, D., Gehrels, N., Baltay, C., et al. 2015, arXiv:1503.03757
- Stark, D. P., Ellis, R. S., Charlot, S., et al. 2017, *Monthly Notices of the Royal Astronomical Society*, 464, 469
- Steidel, C. C., Bogosavljević, M., Shapley, A. E., et al. 2011, *The Astrophysical Journal*, 736, arXiv:1101.2204
- Wisotzki, L., Bacon, R., Blaizot, J., et al. 2016, *Astronomy & Astrophysics*, 587, A98
- Wisotzki, L., Bacon, R., Brinchmann, J., et al. 2018, *Nature*, 562, 229
- Zheng, Z., Cen, R., Trac, H., & Miralda-Escudé, J. 2010, *The Astrophysical Journal*, 716, 574
- Zheng, Z., Cen, R., Weinberg, D., Trac, H., & Miralda-Escudé, J. 2011, *The Astrophysical Journal*, 739, 62
- Zheng, Z.-Y., Wang, J., Rhoads, J., et al. 2017, *The Astrophysical Journal*, 842, L22
- Zitrin, A., Fabris, A., Merten, J., et al. 2015, *The Astrophysical Journal*, 801, 44